

Upper Energy Limit of Heavy Baryon Chiral Perturbation Theory in Neutral Pion Photoproduction

C. Fernández-Ramírez^a, A. M. Bernstein^b

^aGrupo de Física Nuclear, Departamento de Física Atómica, Molecular y Nuclear, Facultad de Ciencias Físicas, Universidad Complutense de Madrid, CEI Moncloa, Avda. Complutense s/n, E-28040 Madrid, Spain

^bLaboratory for Nuclear Science and Department of Physics, Massachusetts Institute of Technology, 77 Massachusetts Ave., Cambridge, MA 02139, USA

Abstract

With the availability of the new neutral pion photoproduction from the proton data from the A2 and CB-TAPS Collaborations at Mainz it is mandatory to revisit Heavy Baryon Chiral Perturbation Theory (HBChPT) and address the extraction of the partial waves as well as other issues such as the value of the low-energy constants, the energy range where the calculation provides a good agreement with the data and the impact of unitarity. We find that, within the current experimental status, HBChPT with the fitted LECs gives a good agreement with the existing neutral pion photoproduction data up to ~ 170 MeV and that imposing unitarity does not improve this picture. Above this energy the data call for further improvement in the theory such as the explicit inclusion of the $\Delta(1232)$. We also find that data and multipoles can be well described up to ~ 185 MeV with Taylor expansions in the partial waves up to first order in pion energy.

Keywords: Chiral perturbation theory, effective field theory, pion photoproduction, heavy baryon

1. Introduction

Chiral Perturbation Theory (ChPT) is an effective field theory (EFT) of Quantum Chromodynamics (QCD) in the low-energy domain where quarks and gluons are confined into hadrons and conventional perturbation theory cannot be directly applied. Due to the spontaneous breaking of chiral symmetry in QCD the π meson appears as a pseudoscalar Nambu-Goldstone boson [1] becoming the carrier of the nucleon-nucleon interaction. However, when fully relativistic spin-1/2 matter fields (i.e. nucleon) are introduced in the theory the exact one-to-one correspondence between the loop expansion and the expansion in small momenta and quark masses is spoiled [2]. This is due to the fact that the nucleon mass M does not vanish in the chiral limit. A consistent power counting scheme known as Heavy Baryon Chiral Perturbation Theory (HBChPT) [3] overcomes this difficulty considering the baryons as heavy (static) sources. For πN scattering and pion photoproduction HBChPT has been successful at describing experimental data in the near threshold region [3, 4]. In this Letter we address the question of how well it works for the latest and most accurate $\vec{\gamma}p \rightarrow \pi^0 p$ data to date [5] and to provide an energy range where HBChPT agrees with the latest pion photoproduction data, — the recently completed Mainz data for the differential cross sections $d\sigma/d\Omega$ and linear polarized photon asymmetries Σ for the $\vec{\gamma}p \rightarrow \pi^0 p$ reaction taken from threshold through the $\Delta(1232)$ region. This was performed with a tagged photon beam with energy bins of 2.4 MeV. We also determined the low-energy constants (LECs)

to see if they are actually constant as the photon energy is increased. The quality of the HBChPT fits $-\chi^2$ per degree of freedom (χ^2/dof)— are also compared to a simple *empirical* benchmark fit, a Taylor expansion of the partial waves. The data in [5] are more accurate than previous experiments and the first measurement of the energy dependence of Σ . This has allowed an extraction of the real parts of the four dominant multipoles for the first time —the S-wave E_{0+} and the three P-wave multipoles $P_{1,2,3}$ (E_{1+} , M_{1+} , M_{1-}). This is a much more significant test of the agreement of HBChPT with experiment. As the photon energy increases and the calculations gradually stop agreeing with experiment we have determined whether or not this is caused by one particular multipole. This information, in addition to the behavior of the low energy constants with photon energy provide clues about what improvements are needed to make the HBChPT calculations more accurate.

2. Theoretical Framework

Due to the symmetry breaking, the S-wave amplitude for the $\gamma p \rightarrow \pi^0 p$ reaction is small in the threshold region, — vanishing in the chiral limit [4]. Additionally, the P-wave amplitude is large and leads to the $\Delta(1232)$ resonance at intermediate energies [6]. Hence, for the $\gamma p \rightarrow \pi^0 p$ reaction the S- and P-wave contributions are comparable even very close to threshold [7] and even D waves have an important early contribution due to the weakness of the S wave [8]. The differential cross section and photon asymmetry can be written in terms of electromag-

Email address: cefera@gmail.com (C. Fernández-Ramírez)

netic responses

$$\frac{d\sigma}{d\Omega}(s, \theta) = \frac{q}{k_\gamma} W_T(s, \theta) \quad (1)$$

$$\Sigma(s, \theta) \equiv \frac{\sigma_\perp - \sigma_\parallel}{\sigma_\perp + \sigma_\parallel} = -\frac{W_S(s, \theta)}{W_T(s, \theta)} \sin^2 \theta \quad (2)$$

where W_T and W_S are the electromagnetic responses, θ is the center of mass scattering angle, k_γ the center of mass photon energy, q the pion momentum in the center of mass, and s the squared invariant mass. The responses W_T and W_S are defined in term of the electromagnetic multipoles:

$$W_T = T_0(s) + T_1(s) \mathcal{P}_1(\theta) + T_2(s) \mathcal{P}_2(\theta) + \dots \quad (3)$$

$$W_S = S_0(s) + S_1(s) \mathcal{P}_1(\theta) + \dots \quad (4)$$

where $\mathcal{P}_j(\theta)$ are the Legendre polynomials in terms of $\cos \theta$, the dots stand for negligible corrections, and

$$T_n(s) = \sum_{ij} \text{Re}\{ \mathcal{M}_i^*(s) T_n^{ij} \mathcal{M}_j(s) \} \quad (5)$$

$$S_n(s) = \sum_{ij} \text{Re}\{ \mathcal{M}_i^*(s) S_n^{ij} \mathcal{M}_j(s) \} \quad (6)$$

where $\mathcal{M}_j(s) = E_{0+}, E_{1+}, E_{2+}, E_{2-}, M_{1+}, M_{1-}, M_{2+}, M_{2-}$. The coefficients T_n^{ij} and S_n^{ij} can be found in Appendix A in [9].

The partial waves (electromagnetic multipoles) are not observables and have to be extracted from the experimental data within a theoretical framework (unless a complete experiment is possible [10]). In this Letter we employ three approaches to describe S and P waves that we present in forthcoming paragraphs: Section 2.1 HBChPT [11, 12]; Section 2.2, Unitary HBChPT (U-HBChPT); and Section 2.3, Empirical. In all cases D waves are incorporated using the customary Born terms. Higher partial waves can be safely dismissed in this energy region [9]. The conventions employed in this Letter and further information on the structure of the observables in terms of the electromagnetic multipoles can be found in [9].

2.1. HBChPT

The explicit formulae for the S and P multipoles to one loop and up to $\mathcal{O}(q^4)$ can be found in [11, 12]. Due to the order-by-order renormalization process six LECs appear: a_1 and a_2 associated with the E_{0+} counter-term:

$$E_{0+}^{ct} = ea_1 \omega m_{\pi^0}^2 + ea_2 \omega^3, \quad (7)$$

where ω is the pion energy in the center-of-mass; b_p associated with the $P_3 \equiv 2M_{1+} + M_{1-}$ multipole together with ξ_1 and ξ_2 associated with $P_1 \equiv 3E_{1+} + M_{1+} - M_{1-}$ and $P_2 \equiv 3E_{1+} - M_{1+} + M_{1-}$, respectively. The c_4 LEC associated with P_1 , P_2 , and P_3 has been taken from [13] where it was determined from pion-nucleon scattering inside the Mandelstam triangle. Some other parameters appear in the calculation, but these are fixed. The full list is: the pion-nucleon coupling constant $g_{\pi N} = 13.1$; the weak pion decay constant $f_\pi = 92.42$ MeV, together with the anomalous magnetic moments of the

proton and neutron, the nucleon axial charge g_A (which we fix using the Goldberger–Trieman relation $g_A = g_{\pi N} f_\pi / M$); and the masses of the particles. The pair (a_1, a_2) LECs are highly correlated, $r(a_1, a_2) = -0.99$ [8, 12], and it is more convenient to use the pair of LECs $(a_+ = a_1 + a_2, a_- = a_1 - a_2)$, where a_+ is the leading order for the counter-term close to threshold ($\omega \simeq m_{\pi^0}$) [8]. Henceforth, five LECs are fitted to the data under this approach: a_+, a_-, ξ_1, ξ_2 , and b_p .

2.2. U-HBChPT

From general principles such as time reversal invariance and unitarity the S wave can be written as the combination of a smooth part and a cusp part [9, 14, 15]

$$\begin{aligned} E_{0+} &= e^{i\delta_0} [A_0 + i\beta q_+ / m_{\pi^+}] ; s > s_{thr}^{(\pi^+ n)} \\ E_{0+} &= e^{i\delta_0} [A_0 - \beta |q_+| / m_{\pi^+}] ; s < s_{thr}^{(\pi^+ n)}, \end{aligned} \quad (8)$$

where δ_0 is the $\pi^0 p$ phase shift (which is very small), \sqrt{s} is the invariant mass, $\sqrt{s_{thr}^{(\pi^+ n)}}$ the invariant mass at the $\pi^+ n$ threshold, q_+ is the π^+ center-of-mass momentum, A_0 is E_{0+} in the absence of the charge exchange re-scattering (smooth part), and $\beta = \text{Re}[E_{0+}(\gamma p \rightarrow \pi^+ n)] \times m_{\pi^+ a}(\pi^+ n \rightarrow \pi^0 p)$ parameterizes the magnitude of the unitary cusp and can be calculated [14] on the basis of unitarity. Eq. (8) takes the static isospin breaking (mass differences) as well as πN scattering to all orders into account. In the electromagnetic sector it includes up to first order in the fine structure constant α . The π^+ center-of-mass momentum, q_{π^+} , is real above and imaginary below the π^+ threshold; this is a unitary cusp whose magnitude is parametrized by β which can be calculated [14] on the basis of unitarity and taking into account a theoretical evaluation of isospin breaking [16], obtaining $\beta = (3.35 \pm 0.08) \times 10^{-3} / m_{\pi^+}$ where $\text{Re} E_{0+}(\gamma p \rightarrow \pi^+ n) = (28.06 \pm 0.27 \pm 0.45) \times 10^{-3} / m_{\pi^+}$ [17] and $a(\pi^+ n \rightarrow \pi^0 p) = (0.1195 \pm 0.0016) / m_{\pi^+}$ [18]. In HBChPT up to one loop and $\mathcal{O}(q^4)$, β is fixed by the imaginary part of E_{0+} —that is parameter-free—providing $\beta_{HBChPT} = 2.71 \times 10^{-3} / m_{\pi^+}$ which is far away from the unitary value. Because of the lack of unitarity of the S-wave amplitude [11] it is customary to substitute the S wave provided by HBChPT by a unitary prescription [9, 11, 12]. However, in this Letter instead of substituting the entire S wave for a prescription we prefer to substitute only the cusp part in E_{0+} from HBChPT by the cusp part of E_{0+} in Eq. (8), keeping the smooth part provided by HBChPT. In this way we keep the E_{0+} counter-term and both HBChPT and U-HBChPT approaches have the same LECs to fit to the data.

2.3. Empirical fit

The empirical fit is parameterization of the S and P waves with a minimal physics input: unitarity in the S wave through the β parameter and the angular momentum barrier. This is accomplished with a Taylor expansion in the pion energy in the center of mass ω up to first order on the smooth part of E_{0+} and P_i/q adding the cusp part in Eq. (8) to the S wave and keeping

the imaginary part of the P waves equal to zero, in summary¹

$$E_{0+} = E_{0+}^{(0)} + E_{0+}^{(1)} \frac{\omega - m_{\pi^0}}{m_{\pi^+}} + i\beta \frac{q_{\pi^+}}{m_{\pi^+}}, \quad (9)$$

$$P_i/q = \frac{P_i^{(0)}}{m_{\pi^+}} + P_i^{(1)} \frac{\omega - m_{\pi^0}}{m_{\pi^+}^2}; \quad i = 1, 2, 3 \quad (10)$$

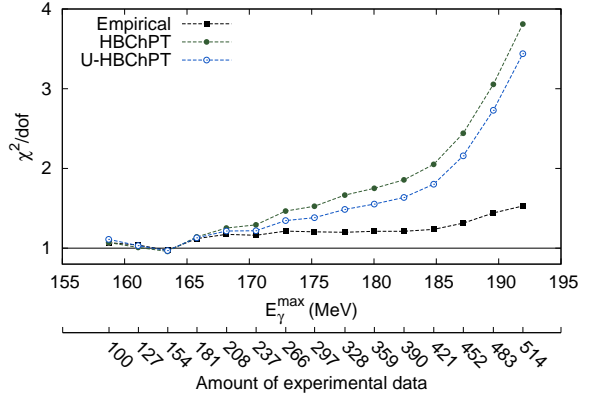
where $E_{0+}^{(0)}$, $E_{0+}^{(1)}$, $P_1^{(0)}$, $P_1^{(1)}$, $P_2^{(0)}$, $P_2^{(1)}$, $P_3^{(0)}$, and $P_3^{(1)}$ are free parameters that will be fitted to the experimental data. We note that this expansion goes to a lesser order in ω than HBChPT – i.e. E_{0+}^{ct} in Eq. (7) goes to order ω^3 – but entails more parameters. We note that chiral symmetry is not imposed in this approach.

3. Results

Equipped with the HBChPT, U-HBChPT and empirical approaches we perform fits to the experimental data in [5] up to different maximum photon energies E_γ^{\max} within the range [158.72, 191.94] MeV and compute the χ^2/dof as well as the corresponding error bars of the extracted parameters (see Appendix A). The energy bins of the data are approximately 2.4 MeV wide, which is taken into account in the fitting and calculations. We do not employ the first two energy bins from [5], 146.95 and 149.35 MeV, because they are less reliable due to systematic errors, starting the fits at $E_\gamma^{\min} = 151.68$ MeV. The amount of data employed in each fit depends on up to what energy we are fitting, — i.e. for our lowest-energy fit ($E_\gamma^{\max} = 158.72$ MeV) we employ 100 experimental data (80 differential cross sections and 20 photon beam asymmetries) and for our highest-energy fit ($E_\gamma^{\max} = 191.94$ MeV) we employ 514 experimental data (360 differential cross sections and 154 photon beam asymmetries). The highest-energy fit has been chosen high enough to obtain a χ^2/dof that ensures that the three approaches no-longer hold and the lowest-energy fit to ensure a reliable fit with enough experimental data. Systematics are not included in the χ^2 and this uncertainty can amount up to 4% in the differential cross section and 5% in the photon asymmetry. The fits are performed employing a genetic algorithm whose details can be found in [19].

3.1. Quality of the fits

Figure 1 shows the χ^2/dof for every fit performed versus the upper energy E_γ^{\max} of the fit as well as the number of data. It is shown that up to ~ 170 MeV all the fits are equally good providing very low χ^2/dof . Above 170 MeV the trend is different; while the empirical fit remains with a good and stable χ^2/dof , both the HBChPT and the U-HBChPT with the fitted LECs start rising, a trend that shows clearly how the theory fails to reproduce the experimental data above that energy. Because we obtain very similar result for U-HBChPT and HBChPT, lack of



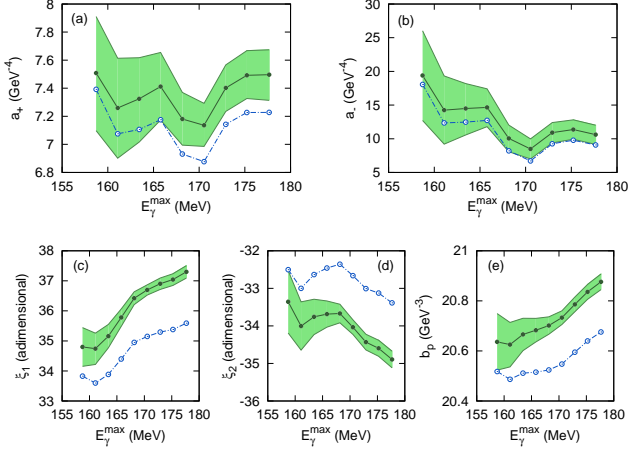


Figure 2: (Color online.) Upper energy (fit) dependence of the LECs. Error band and full circles (green): HBChPT fits; Empty circles (blue): U-HBChPT fit. The high correlation between LECs a_+ and a_- makes their error bars larger. Errorbars for the U-HBChPT LECs are not depicted but they are approximately of the same size as the HBChPT ones.

LECs show that higher order, relativistic and $\Delta(1232)$ effects are absorbed into them, calling for improvement in the theory.

We have also looked into the correlations by computing the correlation coefficient $r(x, y) = \sigma_{xy} / (\sigma_x \sigma_y)$ for each pair of parameters and for every HBChPT and U-HBChPT fit. We find that the correlation remains more or less stable for each pair throughout every fit. The S-wave LECs are highly correlated $r(a_+, a_-) \approx [0.78, 0.88]$, ξ_2 and b_p provide $r(\xi_2, b_p) \approx [0.45, 0.6]$, which is not unexpected due to the photon asymmetry W_S response structure [5, 21], and the rest are fairly uncorrelated lying within the range $[-0.2, 0.2]$. In the case of the S wave the correlation is responsible of the large error bars associated to a_+ and a_- and indicates that energy dependence and threshold value of $\text{Re}E_{0+}$ cannot be obtained separately without further experimental information. Regarding the magnitude of the empirical LECs, the empirical values are within a factor of two of the values estimated in Refs. [11, 12] through resonance saturation.

3.3. Comparison with experimental data

In order to compare with experimental data one has to choose a *best fit* (set of fitted parameters/LECs) for each approach. In our case we pick the fit up to 180.02 MeV for the empirical fit ($\chi^2/\text{dof} = 1.21$) and the fits up to 168.16 MeV for HBChPT ($\chi^2/\text{dof} = 1.25$) and U-HBChPT ($\chi^2/\text{dof} = 1.21$) approaches. Figure 3 shows the single energy multipoles extracted from experimental data compared to the three approaches. The HBChPT fit is shown as an error band. The procedure to obtain the single energy multipoles from the data is explained in [5] and the error bars are computed as described in Appendix A. The data below the unitary cusp (146.95 and 149.35 MeV) are not reliable enough to accurately extract the single energy multipoles and, therefore, are not shown. Overall, the HBChPT and U-HBChPT do a reasonable job describing the multipoles in the whole energy range (up to ~ 185 MeV) except in the case of

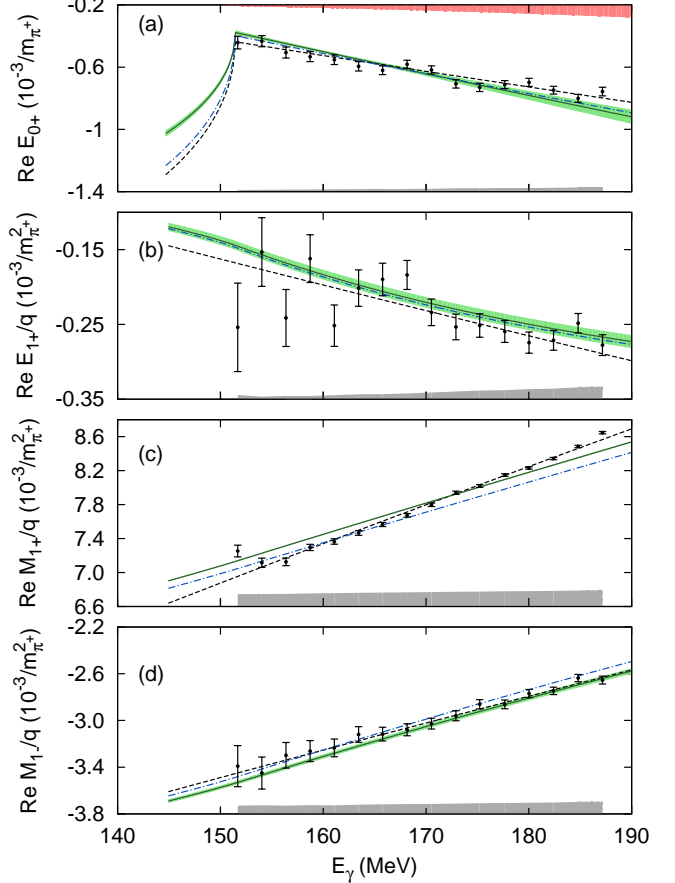


Figure 3: (Color online.) Real part of the S and P waves. HBChPT fit up to 168.16 MeV: Error band and solid line (green); Empirical fit up to 180.02 MeV: Dashed. U-HBChPT fit up to 168.16 MeV: Dash-dotted; The data shown are the single energy multipoles extracted from the experimental differential cross sections and asymmetries in [5]. The gray area above the energy axis represents the systematic errors [5] and the red area at the top of (a) the uncertainty associated to our knowledge of the D waves.

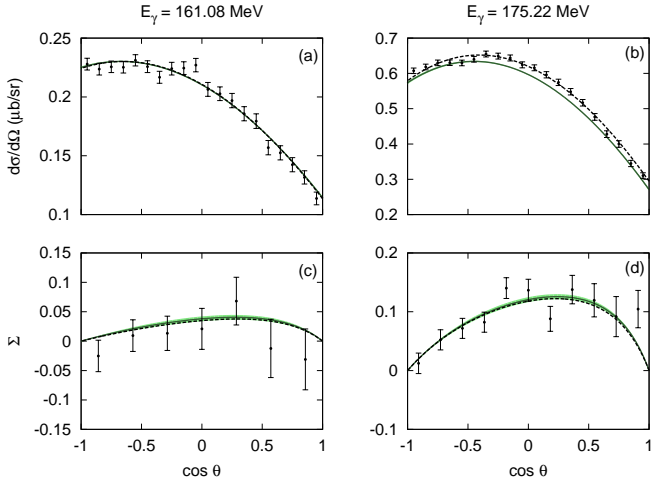


Figure 4: (Color online.) Differential cross section and photon beam asymmetry Σ . Error band and solid line: HBChPT fit up to 168.16 MeV; Dashed: empirical fit up to 180.02 MeV. The U-HBChPT calculation is not depicted because it completely overlaps with the HBChPT. For the photon asymmetry, (c) and (d), the three approaches are undistinguishable.

the M_{1+} , which shows big deviations—specially the slope—between theory and experiment, signaling the necessity to include the $\Delta(1232)$ in the analysis. However, when looking into Figure 3 and comparing fits to extracted single-energy multipoles one has to consider that the error bars for both are computed at the χ^2_1 level as described in Appendix A and the impact of systematics (grey band). Historically the E_{1+} multipole has been considered negligible for many purposes, an approach that is no longer valid due to the achieved experimental accuracy. Moreover, with the current experimental information, the inclusion of a non-zero E_{1+} is mandatory to extract accurately the two other P-wave multipoles. Systematically U-HBChPT P waves are smaller in absolute magnitude than those extracted through HBChPT. This is a consequence of the different β value as explained in Section 3.2. The discrepancy at threshold between HBChPT and unitary fits for $\text{Re}E_{0+}$ is also due to the value of β [9].

Figure 4 compares the empirical, HBChPT and U-HBChPT approaches to the differential cross section and photon beam asymmetry at two different energies, one within the HBChPT and U-HBChPT fitting region ($E_\gamma = 161.08$ MeV) and another outside it ($E_\gamma = 175.22$ MeV). Two results are noteworthy. First, the photon asymmetry is well reproduced for both energies by all the fits, Figures 4.(c) and 4.(d); if we compare with other energies—higher, lower and intermediate—we find the same level of agreement between theory and data, obtaining that all the approaches are of the same quality and provide a good description of the photon asymmetry in the whole energy range considered in this Letter. Second, the HBChPT and U-HBChPT approaches underestimate the cross section for energies above the fitting limit ($E_\gamma^{\text{max}} = 168.16$ MeV), as can be seen in Figure 4.(b). This situation is clearer if we look into the component T_0 of the differential cross section response W_T in Figure 5.(a) which above ~ 170 MeV is largely underestimated by the HBChPT approach. The T_0 component is essentially the

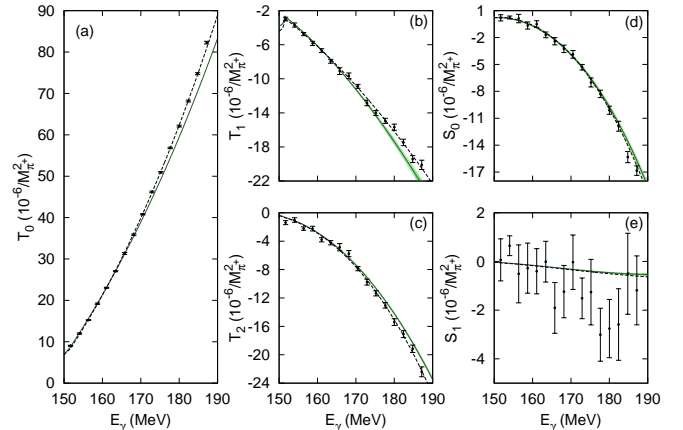


Figure 5: (Color online.) Components of the W_T and W_S responses for the HBChPT fit up to 168.16 MeV (green error band and solid line) and empirical fit up to 180.02 MeV (dashed). All the errors are computed at a $\chi^2 + 1$ level. If the error bars are increased to 2σ the S_1 extraction is compatible with zero in the whole energy range.

total cross section and is dominated by $|M_{1+}|^2$ [9], which as seen in Figure 3, is not so well described by the theory. The significant components of the W_T response T_0 , T_1 , and T_2 are obtained fitting the differential cross sections for each energy bin to Eq. (1). The same operation is done with the photon asymmetry, fitting the data to Eq. (2), extracting S_0 and S_1 . The other two significant components of the W_T response T_1 and T_2 are fairly well described up to ~ 175 MeV. In the case of W_S , S_0 is well determined and HBChPT with the fitted LECs describes it fairly well in the whole energy range.

3.4. Probing D waves

The S_1 component of W_S in Figure 5.(e) is due to the interference among P and D waves [8, 9]. The empirical values of S_1 are consistent with the Born terms contribution of D waves but unfortunately the experiment is not accurate enough in the photon asymmetry to provide a quantitative measurement. The small non-zero effect between 175 and 185 MeV disappears if errors are computed at a 2σ level. Hence, with the current experimental information only four quantities can be accurately obtained from each energy bin T_0 , T_1 , and T_2 from the differential cross section and S_0 from the photon asymmetry, that allows to extract the four multipoles in Figure 3. If we intend to obtain information on the rest of the multipoles we need either more accuracy in the data to pin down S_1 (to obtain information on D waves), T_3 (P×D interference) or T_4 (D waves), or to measure other observables like the target asymmetry (to obtain $\text{Im}E_{0+}$) [21, 22], the E asymmetry [9] (D waves) or the F asymmetry [9, 21, 22] ($\text{Re}E_{0+}$ and D waves). With our current knowledge of the P waves, the accurate extraction of $\text{Im}E_{0+}$ and the β parameter from the target asymmetry is feasible. This observable has been measured at Mainz together with the F asymmetry and data analysis is currently in progress [22].

Returning to D waves, they have been incorporated in our analysis as the Born terms and the S_1 component of W_S is consistent with this approach. Up to order $\mathcal{O}(q^4)$ in HBChPT this

is the only contribution together with an E_{2-} counter-term [23] which provides an additional LEC. However we have neglected it in our calculation because it has no impact in the χ^2 , and, therefore, it cannot be determined. Current experimental information does not allow to test our knowledge on D waves but we are hopeful about forthcoming experiments and we think that future more accurate data will provide a measure of the D-wave effects and allow to pin down the E_{2-} counter-term if a deviation from Born terms is found.

4. Conclusions

Because of the high-quality experimental data gathered by the A2 and CB-TAPS Collaborations at Mainz we can assess the electromagnetic multipoles and their energy dependence to the best precision ever and we can accurately assess the energy range where HBChPT with the fitted LECs provides a good description of the data. Based on the accumulated evidence –LECs stability, χ^2/dof and the empirical fit which works up to ~ 180 MeV– we find that HBChPT with the fitted LECs provides a good description of the experimental data up to 170 MeV. The lack of unitarity in the S wave is not responsible for the disagreement between HBChPT and the experimental data as we have proved through the U-HBChPT approach. The slopes of the P-wave LECs in Figure 2 show how higher order, relativistic and $\Delta(1232)$ effects are absorbed into them, calling for improvement in the theory. Some steps have been taken recently to improve the theory, i.e. Dispersive Chiral Effective Theory [24] which combines dispersion relations with ChPT, and relativistic Chiral Perturbation Theory [23] which does not provide better agreement with data than the HBChPT approach [5]. We have achieved an unprecedented accuracy in our empirical extraction of the multipoles from the data. This has provided a more sensitive test of the HBChPT calculations than has been previously possible. What we have found is that there is a single multipole (M_{1+}) that is causing the gradual deviation from experiment (increasing χ^2) with increasing energy so this disagreement is probably due to the fact that the $\Delta(1232)$ degree of freedom is not being taken into account in a dynamic way [25].

Acknowledgements

We thank the A2 and CB-TAPS Collaborations for making available the experimental data prior to publication. C.F.-R. is supported by “Juan de la Cierva” programme of Spanish Ministry of Economy and Competitiveness and his research has been conducted with support by Spanish Ministry of Economy and Competitiveness grant FIS2009-11621-C02-01, the Moncloa Campus of International Excellence (CEI Moncloa), and by CPAN, CSPD-2007-00042 Ingenio2010. A.M.B. research is supported in part by the US Department of Energy under contract No. DE-FC02-94ER40818.

Appendix A. Error bar calculation

Error bars have been computed through a Monte Carlo (MC) simulation. Once the minimum χ_{\min}^2 has been assessed the χ_1^2 defined as $\chi_1^2 = \chi_{\min}^2 + 1$. Once we have the χ_1^2 we run a MC varying the values of the parameters, we compute the corresponding χ^2 for each set of parameter values, and we accept those sets which provide $\chi^2 \leq \chi_1^2$. If enough statistics are collected, the boundary of the simulation defines the confidence ellipse and the error bars for each parameter [26]. We also obtain correlation plots between parameters as well as the correlation matrix. Once the MC has been run we have a file with thousands of combinations of the parameters which are within the χ_1^2 level. We use those sets to compute the bands in the partial waves and the observables which are shown in the figures. In this way the error bands in the partial waves and the observables take properly into account the correlations among parameters.

References

- [1] J. F. Donoghue, E. Golowich, B. R. Holstein, *Cambridge Monographs in Particle Physics, Nuclear Physics and Cosmology Vol. 2: Dynamics of the Standard Model*, Cambridge University Press, Cambridge 1992.
- [2] J. Gasser, M. E. Sainio, A. Svarc, Nucl. Phys. B 307 (1988) 779.
- [3] V. Bernard, N. Kaiser, U.-G. Meißner, Int. J. Mod. Phys. E 4 (1995) 193.
- [4] V. Bernard, N. Kaiser, J. Gasser, U.-G. Meißner, Phys. Lett. B 268 (1991) 291; V. Bernard, N. Kaiser, U.-G. Meißner, Nucl. Phys. B 383 (1992) 442; V. Bernard, U.-G. Meißner, Annu. Rev. Nucl. Part. Sci., 57 (2007) 33.
- [5] D. Hornidge *et al.*, submitted for publication (2012), arXiv:1211.5495 [nucl-ex].
- [6] A. M. Bernstein, S. Stave, Few Body Syst. 41 (2007) 83.
- [7] A. M. Bernstein, E. Shuster, R. Beck, M. Fuchs, B. Krusche, H. Merkel, H. Ströher, Phys. Rev. C 55 (1997) 1509.
- [8] C. Fernández-Ramírez, A. M. Bernstein, T. W. Donnelly, Phys. Lett. B 679 (2009) 41; C. Fernández-Ramírez, PoS CD09 (2009) 055.
- [9] C. Fernández-Ramírez, A. M. Bernstein, T. W. Donnelly, Phys. Rev. C 80 (2009) 065201.
- [10] I.S. Barker, A. Donnachie, J.K. Storrow, Nucl. Phys. B 95 (1975) 347; W. T. Chiang, F. Tabakin, Phys. Rev. C 55 (1997) 2054.
- [11] V. Bernard, N. Kaiser, U.-G. Meißner, Z. Phys. C 70 (1996) 483.
- [12] V. Bernard, N. Kaiser, U.-G. Meißner, Eur. Phys. J. A 11 (2001) 209.
- [13] P. Büttiker, U.-G. Meißner, Nucl. Phys. A 668 (2000) 97.
- [14] A. M. Bernstein, Phys. Lett. B 442 (1998) 20.
- [15] B. Ananthanarayan, Phys. Lett. B 634 (2006) 391.
- [16] M. Hoferichter, B. Kubis, U.-G. Meißner, Phys. Lett. B 678 (2009) 65.
- [17] E. Korkmaz *et al.*, Phys. Rev. Lett. 83 (1999) 3609.
- [18] V. Baru, C. Hanhart, M. Hoferichter, B. Kubis, A. Nogga, D.R. Phillips, Nucl. Phys. A 872 (2011) 69.
- [19] C. Fernández-Ramírez, E. Moya de Guerra, A. Udías, J. M. Udías, Phys. Rev. C 77 (2008) 065212.
- [20] C. Fernández-Ramírez, arXiv:1304.4855 [nucl-th] (2013).
- [21] A. M. Bernstein, M. W. Ahmed, S. Stave, Y. K. Wu, H. R. Weller, Annu. Rev. Nucl. Part. Sci. 59 (2009) 115.
- [22] D. Hornidge, A.M. Bernstein, Eur. Phys. J.: Special Topics 198 (2011) 133; S. Schumann, AIP Conf. Proc. 1441 (2012) 287; A. M. Bernstein *et al.*, Mainz Exp. A2/10-2009, Measurement of Polarized Target and Beam Asymmetries in Pion-Production on the Proton: Test of Chiral Dynamics (2009).
- [23] M. Hilt, *Photo- and Electro-Pion Production in Chiral Effective Field Theory*, PhD dissertation, University of Mainz (2011); M. Hilt, S Scherer, L. Tiator, Phys. Rev. C 87 (2013) 045204.
- [24] A. Gasparyan, M.F.M. Lutz, Nucl. Phys. A848 (2010) 126.
- [25] T.R. Hemmert, B.R. Holstein, J. Kambor, J. Phys. G 24 (1998) 1831; Phys. Lett. B 395 (1997) 89; V. Lensky, V. Pascalutsa, Eur. Phys. J. C 65 (2010) 195; J. M. Alarcón, J. Martín Camalich, J.A. Oller, Phys. Rev. D

85 (2012) 051503; J. M. Alarcón, J. Martín Camalich, J.A. Oller, *Annals of Physics* (2013), <http://dx.doi.org/10.1016/j.aop.2013.06.001>

[26] J. Beringer *et al.* (Particle Data Group), *Phys. Rev. D* 86 (2012) 010001; G. Cowan, *Statistical Data Analysis*, Oxford University Press, Oxford 2002.